Journal of Marine Science and Technology manuscript No.
(will be inserted by the editor)

Meshfree flat-shell formulation for evaluating linear buckling loads and mode shapes of structural plates

K. Yoshida · S. Sadamoto · Y. Setoyama · S. Tanaka · T.Q. Bui · C. Murakami · D. Yanagihara

Received: date / Accepted: date

Abstract We concentrate our attention on developing a meshfree flat-shell formulation for evaluating linear buckling loads and mode shapes (modes) of structural plates employing an eigen value analysis. A Galerkin-based shear deformable flat-shell formulation for that purpose is proposed. The in-plane and out-of-plane deformations are interpolated using the reproducing kernel particle method (RKPM), while the two membrane deformations, and the three deflection and rotational components are respectively approximated through a plane stress condition and Mindlin-Reissner plate theory. The meshfree discretization by which, as a consequence, constructs five degrees of freedom per node. A generalized eigenvalue problem for the solution of buckling loads and modes of the structural plates is then described. The stiffness matrices of the linear buckling analysis are numerically integrated based on the stabilized conforming nodal integration (SCNI) and subdomain stabilized conforming integration (SSCI). The RKPM and SCNI/SSCI based on Galerkin meshfree formulation, *i.e.*, stabilized meshfree Galerkin method, can overcome the shear locking problem by imposing the Kirchhoff mode reproducing condition. In addition, a singular kernel (SK) function is included in the meshfree interpolation functions to accurately impose the essential boundary conditions. The merits of the developed formulation are demonstrated through numerical buckling experiments of several examples of plates, by which the accuracy and performance of the proposed method are investigated and discussed in detail. It indicates from our numerical results of buckling loads and modes that the proposed meshfree formulation is accurate and useful in the simulation of buckling problems of structural stiffened plates.

Keywords Buckling · Meshfree · FEM · Stiffened Plate

K. Yoshida, S. Sadamoto, Y. Setoyama, S. Tanaka
Graduate School of Engineering, Hiroshima University, 4-1, Kagamiyama 1-chome, Higashi-Hiroshima, 739-8527, Japan
E-mail: satoyuki@hiroshima-u.ac.jp

T.Q. Bui
Department of Civil and Environmental Engineering, Tokyo Institute of Technology, Japan

C. Murakami
National Maritime Research Institute, Japan

D. Yanagihara
Graduate School of Science and Engineering, Ehime University, Japan

1 Introduction

Buckling and ultimate strength evaluations of structural members, e.g., aircraft fuselage, pressure vessel and ship hull, are important to avoid the occurrence of collapse accidents of the structures. The structural members are often composed of rectangular plates, continuous plating and stiffened plate structures. The geometry, plate thickness, aspect ratio and combination of the plates/stiffeners affect the buckling loads, modes and ultimate strength. By enhancing the quality and the performance of the ship structures, their optimum design to avoid or reduce failure problems is essential, by which the studies on buckling behaviors under external and internal loadings play an important role. The buckling loads of several plate structures for ships and marine structures have been analyzed and summarized in common structural rules [1] and recommended practices for marine structures; e.g., [2, 3]. In

addition, advanced evaluations of the buckling and ultimate strength of ship structures have been explored [4–10]. Although flat stiffened plate attached straight stiffeners have often treated, new stiffened plate system including curvilinear shells and curved stiffeners should be taken into account for modern marine structural design.

Shell finite element (FE) modeling has been widely employed to analyze steel plate structures. However, the shear locking problem encountered in the standard finite element method (FEM) formulation has greatly limited its applicability to practical problems. Although several shell formulations and numerical implementations have developed for overcoming the locking problem, see e.g., [11, 12], effective and accurate methods devoted for the solutions of structures with complicated configurations (e.g., plates integrating curved stiffeners) and nonhomogeneous materials (e.g., composite plates) are still required. In the last two decades, meshfree methods and their variant have been introduced and they have successfully applied to solve many engineering problems. These methodologies include the element free Galerkin method [13], reproducing kernel particle method (RKPM) [14–16], meshless local Petrov-Galerkin method [17], moving Kriging meshfree method [18–21] and wavelet Galerkin method [22–26]. Because some of these methods adopt continuous functions as a meshfree interpolant, it is possible to analyze thin-plate structures effectively without encountering shear locking problems. In recent years, isogeometric analysis [27–31] can be used as an alternative method to solve plate bending problems efficiently, because nonuniform rational basis spline (NURBS)-based continuous functions can also be employed as the interpolation function. In this contribution, we particularly focus on buckling analysis of the plate structures with curved stiffeners by a stabilized meshfree Galerkin flat-shell formulation based on the RKPM (stabilized meshfree Galerkin formulation) without shear locking problem.

The RKPM-based Galerkin meshfree plate formulation was originally developed by Wang and Chen [32]. The formulation is based on Mindlin-Reissner plate theory for the treatment of transverse shear stress in plates. The stiffness matrix is numerically integrated using the stabilized conforming nodal integral (SCNI) [33, 34]. A Voronoi cell diagram [35] is adopted for the model generation. The strain components in a Voronoi cell domain are smoothed using the Gauss divergence theorem, and the values are evaluated by nodes in the stabilized numerical integration techniques. The plate bending formulation can possess the Kirchhoff mode reproducing condition (KMRC) [32] on the condition that a complete quadratic basis as the basis vector in the reproducing kernels (RKs) is chosen. To date, the formulation has been applied to geometrical nonlinear analysis by adopting a flat-shell formulation [36, 37], which has five degrees of freedom (DOFs) per node by introducing the plane stress membrane deformation components. In addition, Sadamoto et al. [38] analyzed a large deflection problems of structural plates with initial imperfection using the meshfree formulation by introducing a convected coordinate system. So far, buckling and free vibration problems for un-stiffened plate employing RKPM-based meshfree methods have been solved in [40–42], meshfree analysis for stiffened plate structures including straight and curved stiffeners have not presented yet.

In evaluating the buckling loads and modes of the stiffened plate structures using FEM, stiffened members (e.g., stiffeners, longitudinal girders and transverse frames) are sometimes modeled by suppressing the deflection of the FE model as essential boundary conditions (BCs). There is a steep gradient of displacements and a concentration of stress around the BCs. In the meshfree discretization, sub-domain stabilized conforming integration (SSCI) [39–44] is thus introduced along the BCs to accurately integrate the stiffness matrices for the linear buckling analyses. In the SSCI, a Voronoi cell is further divided into a number of triangles (sub-domains), and SCNI is adopted for each sub-domain. Additionally, a singular kernel (SK) function [45] is introduced to impose the essential BCs and to model the continuous structural plates. An original RK that is located along the boundaries (or edges) and the stiffened members are modified so as to satisfy the Kronecker delta property. The imposition of the essential BCs can be carried out as well as the conventional FEM. Highly accurate and effective enforcement of the essential BCs and modeling of the continuous structures can be achieved.

To date, curved beam problems [46], geometrically nonlinear problems [36–38] and cracked plate problems [47] have been analyzed using the meshfree formulation. Although the flat-shell formulation is attractive for the analysis of buckling loads and modes of the structural plates, buckling analyses of stiffened structural plates have not been reported. Especially, modeling of a plate including curved stiffeners is much more complicated than the straight one, therefore, our target is also to show the applicability of the proposed method. Numerical examples including a square plate, a continuous plate, and a plate with curved stiffeners are considered and analyzed, which are to validate and to show the accuracy, effectiveness and performance of the proposed stabilized meshfree formulation. It is noted that the stiffened members are modeled by suppressing the

deflection components in the meshfree flat-shell modeling.

The paper is organized as follows. Section 2 presents the meshfree approximation of a flat-shell. Section 3 presents the governing equations of the buckling problems and the discretization of the RKs. Numerical examples for buckling analysis of structural plates are considered and the obtained results are investigated and discussed in Section 4. Conclusions drawn from the study are given in the last section.

2 Meshfree approach for a flat-shell

2.1 Representation of a plate deformation

The Mindlin-Reissner plate theory is taken. A schematic of the shear deformable plate is depicted in Fig.1, in which the area of the middle plane, the plate thickness and volume are represented by S, t_h and $V(=S \times t_h)$, respectively.

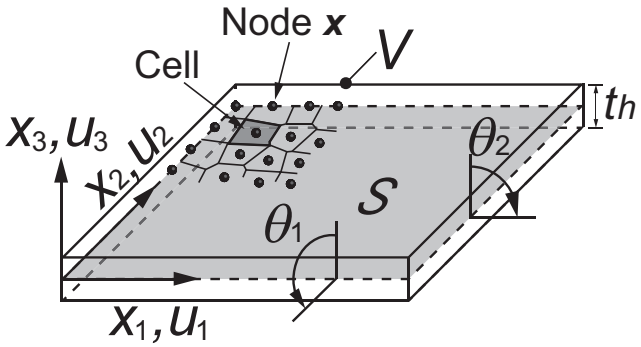

Fig. 1 Geometrical representation of a flat-shell and its meshfree discretization

When solving buckling problems of a plate under a uniaxial thrust, the bending components start to develop stably including the buckling modes above the buckling loads. A flat-shell is thus formulated by coupling with an in-plane deformation and an out-of-plane deformation. In the flat-shell formulation, two DOFs (u_{1mid}, u_{2mid}) for the membrane components plus three DOFs $(u_3, \theta_1, \theta_2)$ for the plate bending components are then considered per node. Here, u_{1mid} and u_{2mid} are membrane displacements in x_1- and x_2-directions in the middle section, respectively, and u_3 is the deflection component of the plate. θ_1 and θ_2 are deflection angles for the x_1- and x_2-axes, respectively. The displacement vector $\boldsymbol{u}(\boldsymbol{x})$ of the shear deformable plate forms

$$\boldsymbol{u}(\boldsymbol{x}) = \begin{Bmatrix} u_1 \\ u_2 \\ u_3 \end{Bmatrix} = \begin{Bmatrix} u_{1mid} + z\theta_2 \\ u_{2mid} - z\theta_1 \\ u_3 \end{Bmatrix}, \tag{1}$$

where u_i (i=1,2,3) represent displacements in a plate along the x_i-axes. And, z ($|z| \leq t_h/2$) represents the plate thickness direction.

2.2 Meshfree RKPM approximation of field variables

In the meshfree discretization, nodes are distributed on the middle-plane of the flat-shell as shown in Fig.1. The RKs are located at each node. The five components u_i (i=1mid, 2mid, 3) and θ_j (j=1,2) are approximated by the RKs. For example, a physical quantity $e(\boldsymbol{x})$ of a plate is represented as

$$e^h(\boldsymbol{x}) = \sum_{I=1}^{NP} \psi_I(\boldsymbol{x}) e_I, \tag{2}$$

where $e^h(\boldsymbol{x})$ is the approximated value and e_I denotes the coefficients. $\boldsymbol{x}$ is a position vector within the analysis domain. NP is the total number of nodes to be used for the approximation. The RK function $\psi_I(\boldsymbol{x})$ is constructed as the sum of the original kernel function $\phi_I(\boldsymbol{x})$ to impose the reproducing condition (RC). The RK function $\psi_I(\boldsymbol{x})$ is represented using a basis vector $\boldsymbol{h}(\boldsymbol{x})$ and the coefficient vector $\boldsymbol{b}(\boldsymbol{x})$ as

$$\psi_I(\boldsymbol{x}) = \boldsymbol{h}^T(\boldsymbol{x}_I - \boldsymbol{x})\boldsymbol{b}(\boldsymbol{x})\phi_I(\boldsymbol{x}_I - \boldsymbol{x}). \tag{3}$$

A cubic spline kernel function [50] is used as the original kernel function $\phi_I(\boldsymbol{x}_I - \boldsymbol{x})$:

$$\phi_I(\boldsymbol{x}_I - \boldsymbol{x}, h) = \frac{10}{7\pi h^2} \begin{cases} 1 - \frac{3}{2}s^2 + \frac{3}{4}s^3 & (0 \leq s \leq 1) \\ \frac{1}{4}(2-s)^3 & (1 \leq s \leq 2) \\ 0 & (2 \leq s) \end{cases}, \tag{4}$$

where s ($=|\boldsymbol{x}_I - \boldsymbol{x}|/h$) is the normalized distance from the center of the kernel, and h is a parameter that determines the function support.

The RC in the two-dimensional (2D) case is expressed as

$$\sum_{I=1}^{NP} \psi_I(\boldsymbol{x}) x_{1I}^i x_{2I}^j = x_1^i x_2^j, \quad (0 \leq i+j \leq 2), \tag{5}$$

which can be rewritten in vector form as

$$\sum_{I=1}^{NP} \psi_I(\boldsymbol{x}) \boldsymbol{h}(\boldsymbol{x}_I - \boldsymbol{x}) = \boldsymbol{h}(\boldsymbol{0}). \tag{6}$$

Substituting Eq.(3) into Eq.(6), a simultaneous linear equation is obtained,

$$\boldsymbol{M}(\boldsymbol{x})\boldsymbol{b}(\boldsymbol{x}) = \boldsymbol{h}(\boldsymbol{0}), \tag{7}$$

where $\boldsymbol{M}(\boldsymbol{x})$ is a moment matrix,

$$\boldsymbol{M}(\boldsymbol{x}) = \sum_{I=1}^{NP} \boldsymbol{h}(\boldsymbol{x}_I - \boldsymbol{x})\boldsymbol{h}^T(\boldsymbol{x}_I - \boldsymbol{x})\phi_I(\boldsymbol{x}_I - \boldsymbol{x}). \quad (8)$$

The coefficient vector $\boldsymbol{b}(\boldsymbol{x})$ is obtained by analyzing Eq.(7). Eq.(3) can be rewritten as

$$\psi_I(\boldsymbol{x}) = \boldsymbol{h}^T(\boldsymbol{0})\boldsymbol{M}^{-1}(\boldsymbol{x})\boldsymbol{h}(\boldsymbol{x}_I - \boldsymbol{x})\phi_I(\boldsymbol{x}_I - \boldsymbol{x}). \quad (9)$$

When a complete quadratic basis is used as the basis vector $\boldsymbol{h}(\boldsymbol{x})$ in the RKs, a pure bending mode can be expressed in the meshfree Mindlin-Reissner plate formulation; i.e., $\boldsymbol{h}^T(\boldsymbol{x})$=$\{1\ x_1\ x_2\ x_1^2\ x_1x_2\ x_2^2\}$. This makes it possible for possessing the KMRC, and a highly accurate meshfree analysis can be carried out without the shear locking problem. The details of the KMRC can be found in [32, 37, 39].

2.3 SK function

It is known that meshfree interpolants based on moving-least-square or RK approximations do not have the Kronecker delta property; i.e., $d^h(\boldsymbol{x})\neq d_I$ in Eq.(2). This thus induces difficulties in imposing the essential BCs in meshfree methods. Chen and Wang [45] proposed a SK function for correcting original RK to satisfy the Kronecker delta property. Here, we briefly summarize the SKs.

The original kernel function $\phi_I(\boldsymbol{x}_I - \boldsymbol{x})$ in Eq.(4) is modified for introducing a singularity associated with a designated node J located at $(\hat{x}_{1J}, \hat{x}_{2J})$ on the boundary:

$$\hat{\phi}_J(\hat{x}_{1J} - x_1, \hat{x}_{2J} - x_2) = \frac{\phi_J(\hat{x}_{1J} - x_1, \hat{x}_{2J} - x_2)}{f(\hat{x}_{1J} - x_1, \hat{x}_{2J} - x_2)}, \quad (10)$$

where ($\hat{}$) represents a node imposed singularity in an associated kernel function. The function $f(\hat{x}_{1J} - x_1, \hat{x}_{2J} - x_2)$ is expressed as

$$f(\hat{x}_{1J} - x_1, \hat{x}_{2J} - x_2) = \left[\left(\frac{\hat{x}_{1J} - x_1}{p}\right)^2 + \left(\frac{\hat{x}_{2J} - x_2}{p}\right)^2\right]^c, \quad (11)$$

where p (=$2h$) is a parameter that determines the function support. The parameter c is the order of the singularity and values of 0.1 to 2.0 have been suggested [45]; c=1.0 is chosen in the present study. The RKs associated with the SK function are expressed as

$$\hat{\psi}_J(\boldsymbol{x}) = \boldsymbol{h}^T(\boldsymbol{0})\hat{\boldsymbol{M}}^{-1}(\boldsymbol{x})\boldsymbol{h}(\hat{\boldsymbol{x}}_J - \boldsymbol{x})\hat{\phi}_J(\hat{\boldsymbol{x}}_J - \boldsymbol{x}), \quad (12)$$

$$\hat{\boldsymbol{M}}(\boldsymbol{x}) = \left[\sum_{I=1, I\neq J}^{NP} \boldsymbol{h}(\boldsymbol{x}_I - \boldsymbol{x})\boldsymbol{h}^T(\boldsymbol{x}_I - \boldsymbol{x})\phi_I(\boldsymbol{x}_I - \boldsymbol{x})\right] + \boldsymbol{h}(\hat{\boldsymbol{x}}_J - \boldsymbol{x})\boldsymbol{h}^T(\hat{\boldsymbol{x}}_J - \boldsymbol{x})\hat{\phi}_J(\hat{\boldsymbol{x}}_J - \boldsymbol{x}). \quad (13)$$

Figs.2a and b show examples of the original RK function and the SK function, respectively. The essential BCs can be accurately imposed by introducing the SK function in the meshfree modeling. The SK function set for imposing the essential BCs. The error in the essential BCs is close to zero to the limit of machine precision.

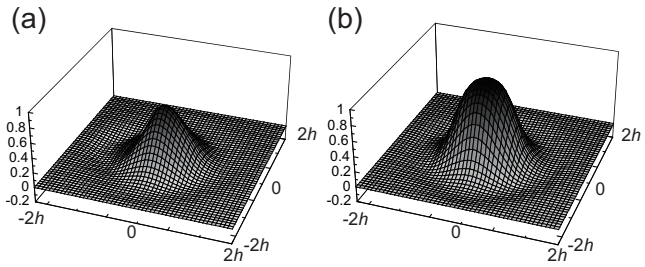

Fig. 2 RK functions. **a** An original RK function. **b** A SK function

3 A flat-shell formulation for linear buckling analysis

3.1 Governing equations and a weak-form

A flat-shell is analyzed employing the meshfree Galerkin formulation for the buckling loads and modes evaluations of structural plates. The body force term is not included in the formulation. The virtual work principle can be written as

$$\int_V \boldsymbol{\sigma} : \delta\boldsymbol{\varepsilon}\ dV = \int_S \bar{\boldsymbol{t}} \cdot \delta\boldsymbol{u}\ dS. \quad (14)$$

$\boldsymbol{\sigma}$ and $\boldsymbol{\varepsilon}$ are the Cauchy stress tensor and strain tensor, V is the volume of the plates. The term δ represents their variation. $\bar{\boldsymbol{t}}$ is the traction force vector applied to the body on the traction boundary S. The numerical integration of the linear formulation in Eq.(14) is performed with the meshfree approximation and the nodal integration techniques SCNI/SSCI presented in section 3.2.

3.2 Nodal integration techniques

In the meshfree discretization, nodes are distributed on the middle plane of the flat-shell. A Voronoi cell is automatically generated according to the nodes as denoted

in Fig.3. $\boldsymbol{x}_K$ denotes the coordinates of the K-th node. Ω_K is the area of the Voronoi cell, and Γ_K is its boundary. $\boldsymbol{n}$ is normal to the cell. SCNI and SSCI are employed for the numerical integration of the Galerkin meshfree formulation. The five DOFs are denoted as $\{u_{1mid}\ u_{2mid}\ u_3\ \theta_1\ \theta_2\}^T=\{d_1\ d_2\ d_3\ d_4\ d_5\}^T$.

When adopting SCNI, the derivatives of the components for $\tilde{d}^h_j(\boldsymbol{x}_K)$ $(j=1,\cdots,5)$ are represented as

$$\tilde{d}^h_{j,k}(\boldsymbol{x}_K) = \frac{1}{A_K}\int_{\Omega_K} d^h_{j,k}(\boldsymbol{x}_K)\, d\Omega = \sum_{I=1}^{NP} b_{Ik}(\boldsymbol{x}_K) d_{jI},\ \ k=\{1,\ 2\}, \tag{15}$$

where $\tilde{d}^h_{j,k}(\boldsymbol{x}_K)$ denotes differentiations for the x_k-axis (k=1,2), and A_K is the area of Ω_K. ($\tilde{}$) represents smoothed physical quantities evaluated using the nodal integration techniques. The scalar value $b_{Ik}(\boldsymbol{x}_K)$ is evaluated using a line integral as

$$b_{Ik}(\boldsymbol{x}_K) = \frac{1}{A_K}\int_{\Gamma_K} \psi_I(\boldsymbol{x}) n_k\, d\Gamma,\ \ k=\{1,\ 2\}. \tag{16}$$

n_k denotes the x_1- and x_2-components of the normal vector. The physical values of SCNI are evaluated at each node.

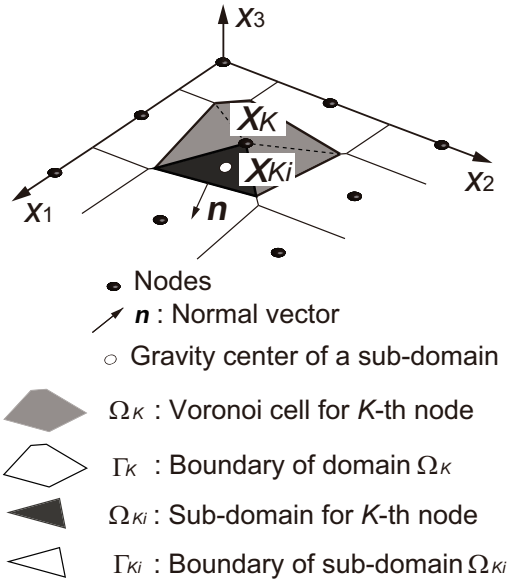

Fig. 3 A schematic illustration of nodal integration techniques SCNI/SSCI

When solving linear buckling problems of plate structures including stiffeners or crack defects, an improved hybrid numerical integration scheme is needed to accurately derive stiffness matrix along stiffeners lines or crack lines because high stress gradients [37,52] and displacement discontinuities sometime occur [47–49]. SSCI [39–44] is also introduced to the nodes of BCs. The integration area of SCNI Ω_K is further divided into a number of triangular areas (sub-domains) Ω_{K_i} as shown in Fig.3. Additionally, SCNI is adopted for each sub-domain. The physical values are evaluated at the gravity center $\boldsymbol{x}_{K_i}$. In SSCI, differentiations $\tilde{d}^h_{j,k}(\boldsymbol{x}_{K_i})$ of the components $\tilde{d}^h_j(\boldsymbol{x}_{K_i})$ are expressed as

$$\tilde{d}^h_{j,k}(\boldsymbol{x}_{K_i}) = \frac{1}{A_{K_i}}\int_{\Omega_{K_i}} d^h_{j,k}(\boldsymbol{x}_{K_i})\, d\Omega = \sum_{I=1}^{NP} b_{Ik}(\boldsymbol{x}_{K_i}) d_{jI},\ \ k=\{1,\ 2\}, \tag{17}$$

where the scalar value $b_{Ik}(\boldsymbol{x}_{K_i})$ is expressed as

$$b_{Ik}(\boldsymbol{x}_{K_i}) = \frac{1}{A_{K_i}}\int_{\Gamma_{K_i}} \psi_I(\boldsymbol{x}) n_k\, d\Gamma,\ \ k=\{1,\ 2\}. \tag{18}$$

A_{K_i} is the area of Ω_{K_i}, and n_k denotes the normal vector components $\boldsymbol{n}$ for the boundary of the sub-domains Γ_{K_i}. When evaluating a line integration in Eqs.(16) and (18), the five-point Gauss quadrature is adopted.

In terms of the flat-shell formulation, rotational components and the derivative of the deflection components are included in the shear strain term. In the discretization, SCNI/SSCI is adopted for the derivative of the deflection components, and a surface integral is directly adopted for the rotational components as presented in [47]. A Voronoi cell is further divided into a number of triangles, and the 13-point Gauss quadrature is applied to each triangle in the surface integral.

3.3 Discretization for linear buckling analysis

When considering an elastic stability problem of shear deformable plate, the linear formulation of Eq.(14) is represented as

$$\int_V \boldsymbol{\sigma} : \delta\boldsymbol{\varepsilon}_{\mathrm{L}} dV + \lambda \int_V \boldsymbol{\sigma}'_0 : \delta\boldsymbol{\varepsilon}_{\mathrm{NL}} dV = 0, \tag{19}$$

where $\boldsymbol{\varepsilon}_{\mathrm{L}}$ and $\boldsymbol{\varepsilon}_{\mathrm{NL}}$ are the linear and nonlinear parts of strain tensors, respectively. $\boldsymbol{\sigma}'_0$ is the pre-buckling stress tensor, and λ is the buckling factor. The linear strain components $\varepsilon_{\mathrm{L}ij}$ $(=\boldsymbol{\varepsilon}_{\mathrm{L}})$ can be described as

$$\begin{Bmatrix} \varepsilon_{\mathrm{L}11} \\ \varepsilon_{\mathrm{L}22} \\ 2\varepsilon_{\mathrm{L}12} \\ 2\varepsilon_{\mathrm{L}31} \\ 2\varepsilon_{\mathrm{L}23} \end{Bmatrix} = \begin{Bmatrix} \frac{\partial u_{1mid}}{\partial x_1} + z\frac{\partial \theta_2}{\partial x_1} \\ \frac{\partial u_{2mid}}{\partial x_2} - z\frac{\partial \theta_1}{\partial x_2} \\ \frac{\partial u_{1mid}}{\partial x_2} + \frac{\partial u_{2mid}}{\partial x_1} + z\left(\frac{\partial \theta_2}{\partial x_2} - \frac{\partial \theta_1}{\partial x_1}\right) \\ \frac{\partial u_3}{\partial x_1} + \theta_2 \\ \frac{\partial u_3}{\partial x_2} - \theta_1 \end{Bmatrix}. \tag{20}$$

The nonlinear strain tensor $\boldsymbol{\varepsilon}_{\mathrm{NL}}$ is defined as

$$\varepsilon_{\mathrm{NL}ij} = \frac{1}{2}\left(\frac{\partial u_i}{\partial x_i}\frac{\partial u_i}{\partial x_j}\right). \tag{21}$$

Eq.(19) is decomposed by constitutive and strain displacements relations. And, it is discretized as

$$\left[\int_V \boldsymbol{B}_{\mathrm{L}}^T \boldsymbol{C}\boldsymbol{B}_{\mathrm{L}} dV + \lambda \int_V \boldsymbol{B}_{\mathrm{NL}}^T \boldsymbol{\sigma}_0' \boldsymbol{B}_{\mathrm{NL}} dV\right]\boldsymbol{U} = 0, \tag{22}$$

where $\boldsymbol{B}_{\mathrm{L}}$ and $\boldsymbol{B}_{\mathrm{NL}}$ are displacement-strain matrices in the meshfree model, and $\boldsymbol{C}$ is the stress-strain relationship. Finally, a generalized eigenvalue problem for the linear buckling analysis can be derived based on Eq.(22) as

$$(\boldsymbol{K}_{\mathrm{L}} + \lambda \boldsymbol{K}_{\mathrm{NL}})\boldsymbol{U} = 0. \tag{23}$$

$\boldsymbol{U}$ is the buckling mode which corresponds to λ. Because the geometrical stiffness matrix $\boldsymbol{K}_{\mathrm{NL}}$ is a non-regular matrix, following equation is then analyzed

$$(\frac{1}{\lambda}\boldsymbol{K}_{\mathrm{L}} + \boldsymbol{K}_{\mathrm{NL}})\boldsymbol{U} = 0. \tag{24}$$

The buckling loads and modes of the meshfree model can be obtained by solving Eq.(24).

4 Numerical examples and discussion

In this section, several numerical examples of buckling problems including square plates, continuous plating, and rectangular plate with curved stiffeners are considered and investigated. In the meshfree modeling, the stiffeners, longitudinal girders and transverse frames are located on nodes and modeled by suppressing the deflection components of the nodes. SSCI is adopted for Voronoi cells belong to the nodes. For verification purpose, apart from the example whose analytical solutions are available, other reference solutions are derived from the use of the commercial FEM software (MSC.Marc). Four-node-thick quadrilateral shell elements (element number : 75) is used. Although the first and second buckling loads and modes in general are required for the examination of buckling behaviors of the structural plates, higher orders are also analyzed to show the accuracy of the proposed meshfree formulation and discretization.

4.1 A square plate

We start by considering a square plate under biaxial loads as depicted in Fig.4a with several BCs. The dimensions of the plate are a=b=1,000 mm, and the plate thickness is t_h=10 mm. Young's modulus is E=205.8 GPa and Poisson's ratio is ν=0.3. The effects of the boundary and loading conditions on the buckling loads are analyzed, and the obtained numerical results are then compared against the analytical reference solutions [51] and the FEM results. The BCs sketched in Fig.4a are defined as follows. The terms "S" and "C" indicate the simply supported and fully clamped BCs, respectively. "S" and "C" are imposed on the four edges (i), (ii), (iii) and (iv) as shown in Fig.4a. In the case of SCSC, for example, edges (i) and (iii) are simply supported whereas the edges (ii) and (iv) are fully clamped. Six BCs are considered: SSSS, CCCC, SCSC and CSCS under uniaxial compressive loads in the x_1-direction and SSSS and CCCC under biaxial compressive loads in the x_1- and x_2-directions. A total of 625 (25×25) scattered nodes are employed for the regular and irregular meshfree models. The distribution of nodes and Voronoi cell diagrams are presented in Figs.4b and c. SCNI is only employed for the nodal integration of the stiffness matrices.

Table 1 presents a comparison of the numerical results of buckling factor k=$\lambda b/(D\pi^2)$ among the regular/irregular distributed models, analytical solutions [51], and the FEM. D=$Et^3/12(1-\nu^2)$ is the flexural rigidity. The errors η % between meshfree and analytical solutions are also represented in Table 1. 1,600 (40×40) equally spaced FEs are used in the FE analyses. The numerical results are in good agreement with the analytical and reference solutions in all cases for the several boundary and loading conditions. It is very interesting to see that the influence of the irregular meshfree discretization on the buckling factor is insignificant. This implies that the proposed formulation is insensitive to the irregularly scattered distribution. We also report the percentage errors estimated over the analytical solutions given in parenthesis for the developed meshfree and FEM method. High accuracy of the present meshfree formulation is observed.

4.2 A continuous plate structure

Next example deals with a continuous plate structure as shown in Fig.5a. A continuous flat-shell plate is suppressed by longitudinal stiffeners and transverse frames. The distance between adjacent transverse frames is a, and the distance between longitudinal stiffeners is b. Three meshfree models with a=400, 1,200 and 2,000 mm and b=400 mm are developed. The aspect ratio a/b is 1.0, 3.0 and 5.0, respectively. The plate thickness t_h is assumed to be 10 mm. Young's modulus is E=205.8 GPa and Poisson's ratio is ν=0.3. The shaded region (IJKL) in Fig.5a (i.e., triple-span) is modeled to

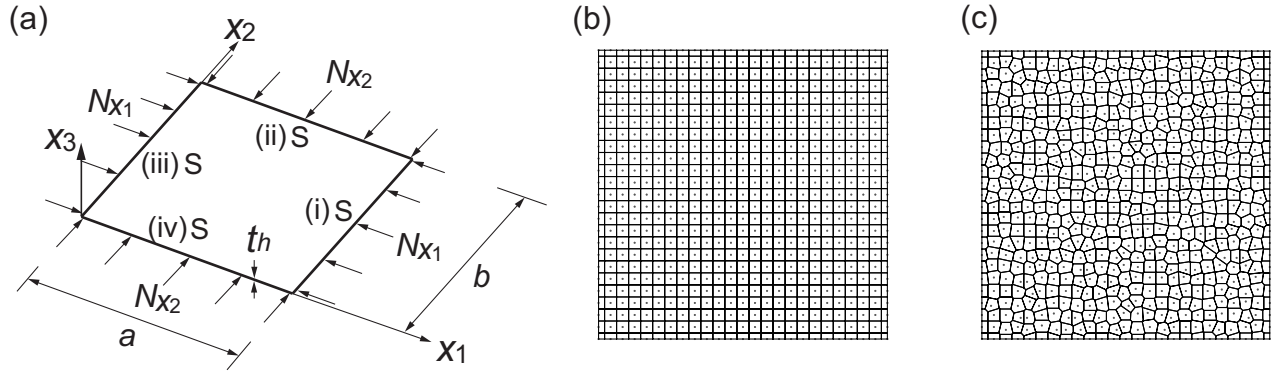

Fig. 4 A schematic illustration of a square plate and the meshfree discretization. **a** Loading and boundary conditions (SSSS). **b** Regular model. **c** Irregular model

Table 1 Comparison of the buckling factor k of a square plate among the analytical, FEM and the present formulation methods and their errors

Loading conditions	BCs	Analytical solution [51]	Regular	Irregular	FEM	η (%) (Regular)	η (%) (Irregular)
N_{x_1}	SSSS	4.00	3.9818	3.9754	3.9803	0.46	0.62
N_{x_1}	CCCC	10.07	10.0019	10.0222	10.0678	0.68	0.48
N_{x_1}	SCSC	7.69	7.6401	7.6399	7.6596	0.65	0.65
N_{x_1}	CSCS	6.74	6.7239	6.7204	6.7301	0.24	0.29
$N_{x_1} = N_{x_2}$	SSSS	2.00	1.9909	1.9878	1.9902	0.46	0.61
$N_{x_1} = N_{x_2}$	CCCC	5.33	5.2839	5.2844	5.3012	0.87	0.86

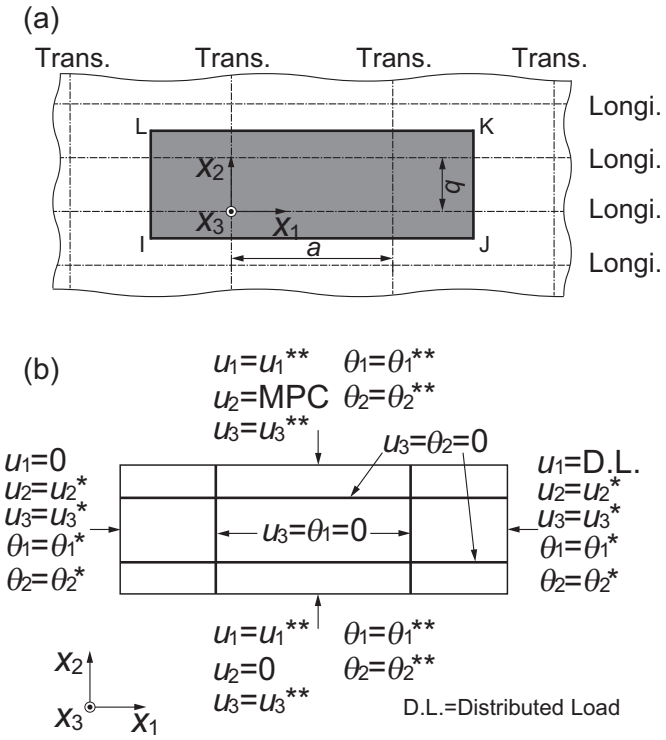

Fig. 5 Model of a continuous plating. **a** Triple-span model. **b** Boundary conditions of the continuous plate

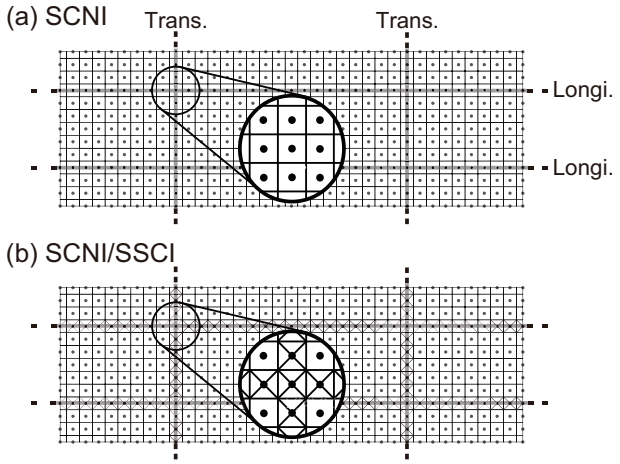

Fig. 6 Node distribution and domains for the nodal integrations (a/b=3.0). **a** Full SCNI model. **b** SCNI/SSCI hybrid model

examine the accuracy and effectiveness of the meshfree modeling, although the buckling loads and modes are equivalent to the results for a rectangular plate, if the continuous plate is assumed to be simply supported along longitudinal stiffener and transverse frame lines. To ensure continuity of the plating, the in-plane displacement of the edges in perpendicular directions is considered to be uniform, and periodical BCs are imposed as shown in Fig.5b.

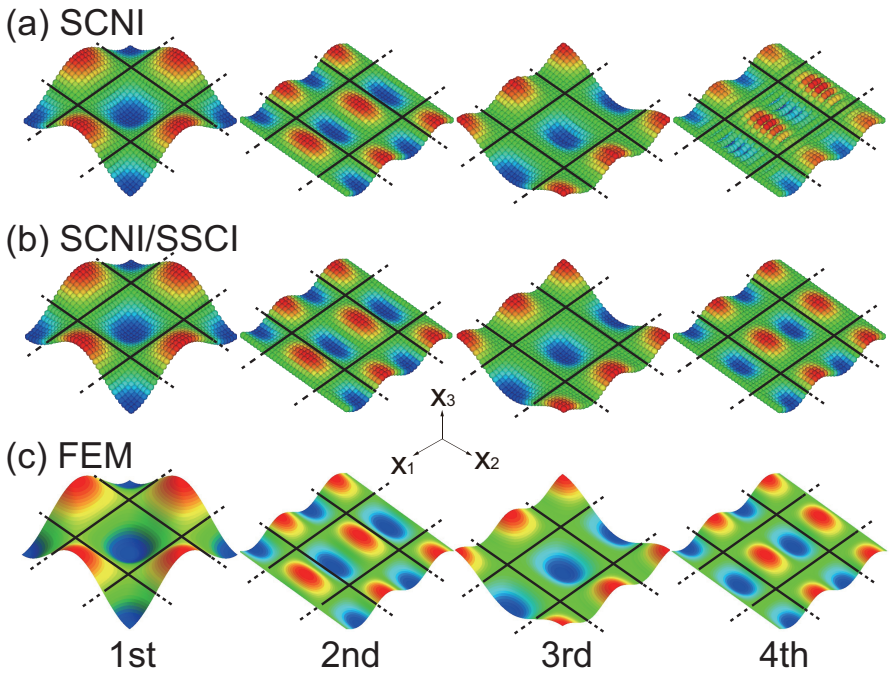

Fig. 7 Comparison of the first four buckling modes of the continuous plate (a/b=1.0). **a** Full SCNI model. **b** SCNI/SSCI hybrid model. **c** FEM

Two kinds of meshfree models are employed to examine the accuracy of the nodal integration techniques for integrating the stiffness matrices. One is the full SCNI model, and the other is the SCNI/SSCI hybrid model. For example, meshfree models having an aspect ratio a/b=3.0 are presented in Figs.6a and b. They have 37×13 nodes, and the node distance is α=200/3 mm. The full SCNI model is employed SCNI throughout the analysis domain. In the SCNI/SSCI hybrid model, Voronoi cells along the transverse frames and longitudinal girders are divided into a number of triangular sub-domains, and SSCI is employed. The buckling loads and modes are compared with the FE results using the MSC.Marc.

The first four buckling modes (a/b=1.0) are depicted in Figs.7a, b and c, which are accounted by using the full SCNI, SCNI/SSCI hybrid and FE models, respectively. Although the first to third buckling modes of the meshfree models are consistent with those of the reference solutions, an oscillation in the buckling mode can be observed in the fourth buckling mode of the full SCNI model as shown in Fig.7a. The buckling stresses calculated by the meshfree models are presented in Table 2. There is also a slight difference between the results of the full SCNI model and the FE results in the fourth buckling stress. Meanwhile, the results of the SCNI/SSCI hybrid are in good agreement with the reference solutions. A similar tendency is found for the higher order buckling loads and modes.

In the author's previous study [52], a similar oscillation in the deflection can be seen in the linear analysis of plate bending problems, when the full SCNI model is adopted and the deflection of the flat plate is suppressed locally. The full SCNI model thus cannot represent accurately the local deformation because the stress/strain components are smoothed throughout the cell. Meanwhile, the combination of SCNI and SSCI provides good agreement with the reference solutions since the local deformation can be represented by subdividing a Voronoi cell into sub-domains for SSCI along the stiffened members.

To further examine linear buckling analysis with the SCNI/SSCI hybrid model, a convergence study is carried out for the first buckling stresses of the meshfree models with a/b=1.0, 3.0 and 5.0. The error η % is defined as

$$\eta = \left| \frac{\sigma_{cr.} - \sigma_{ref.}}{\sigma_{ref.}} \right| \times 100\ (\%), \tag{25}$$

where $\sigma_{cr.}$ and $\sigma_{ref.}$ are the critical buckling stresses obtained from the meshfree modeling and FE results. A fully converged FE solution is employed for the reference solutions. The convergence results derived from the present formulation are shown in Fig.8. The results are also compared with the FEM results. α is a node spacing of the meshfree and FEM models. The solutions of the meshfree method and FEM monotonically converge as the node spacing decreases. When coarse

models employed in the meshfree method, the results with FEM are superior to those of the meshfree ones. This is because the function support of the meshfree interpolation function is wider than the FEM bilinear function. Therefore, meshfree results with the coarse model are sensitive to the boundary condition. While the convergence rates of the present formulation is superior to those of the FEM. It is thus confirmed that the meshfree modeling and nodal integration techniques SCNI/SSCI for continuous plating work well.

Table 2 Comparison of the buckling stress $\sigma_{cr.}$ for continuous plates (α=200/3 mm)

(N/mm^2)	1st	2nd	3rd	4th
SCNI	462.17	715.80	771.16	810.77
SCNI/SSCI	462.53	725.13	771.76	881.88
FEM	463.69	721.49	778.73	884.43

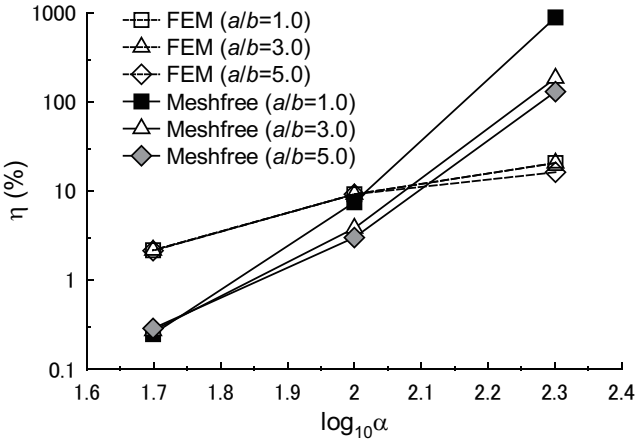

Fig. 8 Convergence study for the continuous plates with different aspect ratio a/b (SCNI/SSCI hybrid model and FEM)

4.3 A rectangular plate with curved stiffeners

To demonstrate the advantage of the proposed meshfree modeling, buckling analyses of a rectangular plate with curved stiffeners are performed. Such a structural model is sometimes adopted in aerospace, marine engineering and architecture constructions. Although there are difficulties in generating the FE models, it is relatively easy to make the meshfree models because the nodes can easily be located along the curved stiffeners. Rectangular plate models including one and two curved stiffeners analyzed in Refs. [53, 54] are taken as examples, and the buckling modes and loads are evaluated.

4.3.1 One curved stiffener

A rectangular plate with a curved stiffener is analyzed. Two kinds of curved stiffener models are chosen. The models are respectively called Models A and B, and they are represented in Figs.9a and b. The dimensions of the rectangular plate are a=b=120 mm. The plate thickness t_h is 1.2 mm. The material properties are E=69 GPa and ν=0.3. The curved stiffeners are expressed by polynomial equations as x_2=0.0176$(x_1 - 50)^2 + 30$ mm in the case of Model A, and x_2=$-5.5 \times 10^{-3}x_1^2 + 0.7x_1 + 40$ mm in the case of Model B.

Meshfree versions of Models A and B are represented in Figs.9c and d. They have 1,683 and 1,685 nodes, respectively. Voronoi cells are generated throughout the meshfree models, and SCNI is adopted. SSCI is also adopted along the curved stiffeners. As the BCs, all the edges are assumed to remain straight and be simply supported in both cases and subjected to biaxial compression loads. To provide reference solutions, linear buckling analysis is carried out using the FEM. The FE models have 16,121 and 12,923 elements, respectively.

The first four buckling factors k of Models A and B are presented in Table 3, and their buckling modes are visualized in Figs.10 and 11. FE results are also presented. Although the buckling modes are slightly complicated compared with those of the rectangular plate without stiffeners, the buckling loads and modes obtained with meshfree modeling are in good agreement with the reference solutions.

Table 3 Comparison of the buckling factor k of rectangular plates with a curved stiffener for Models A and B between the present meshfree method and FEM

Model		1st	2nd	3rd	4th
A	Meshfree	5.3780	9.6392	10.6699	13.1084
	FEM	5.4137	9.6241	10.7243	13.0765
B	Meshfree	5.2060	8.2751	8.6687	10.9791
	FEM	5.2118	8.2695	8.6904	11.0425

4.3.2 Two curved stiffeners

To analyze a more complicated geometry employing the meshfree modeling, a rectangular plate with two curved stiffeners is analyzed. The model is called Model C, and it is depicted in Fig.12a. The equations of the two curved stiffeners are x_2=$\sqrt{720^2 - (x_1 - 700)^2} - 100$ mm and x_2=$\sqrt{720^2 - (x_1 + 93.1)^2} - 100$ mm. The material properties are E=73 GPa and ν=0.33. The plate thickness is t_h=4.0 mm. The dimensions of the plate are

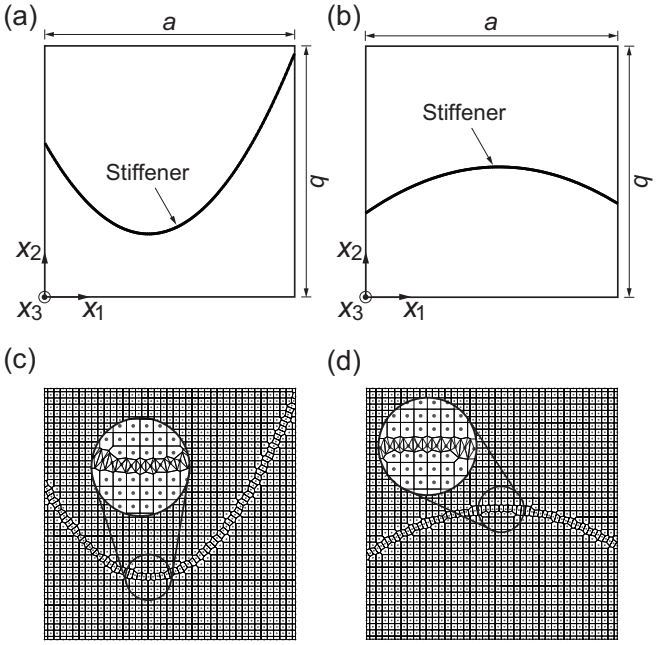

Fig. 9 Rectangular plate with a curved stiffener **a** Model A. **b** Model B. **c** Meshfree model for Model A. **d** Meshfree model for Model B

a=606.9 mm and b=711.2 mm. The boundary and loading conditions are the same as those of Models A and B. Fig.12b shows the node distribution and Voronoi cell diagram. The meshfree model has 1,600 nodes and the FEM model has 9,911 elements. The buckling stresses $\sigma_{cr.}$ from the first to the fourth order buckling stresses are presented in Table 4. The buckling modes are shown in Fig.13. These meshfree results are also in good agreement with the reference solutions.

Table 4 Comparison of the buckling stress $\sigma_{cr.}$ of a rectangular plate with two curved stiffeners (Model C)

(N/mm^2)	1st	2nd	3rd	4th
Meshfree	69.823	129.690	140.871	195.806
FEM	70.057	130.246	141.453	196.270

5 Conclusion

A stabilized meshfree Galerkin flat-shell formulation without shear-locking effect was introduced to solve buckling problems of plate structures. In the meshfree modeling, RKPM and SCNI/SSCI are employed to evaluate the buckling loads and modes effectively. The validity of the proposed approach is verified with several numerical examples for a square plate, a continuous plate, and a plate with one or two curved stiffeners. The numerical results obtained by the present meshfree method are in good agreement with the reference solutions. The buckling of a complex geometry can thus be analyzed employing the meshfree model. Once again, the numerical results indicate that an oscillation in the buckling modes can be found when the full SCNI-based meshfree is taken, whereas the hybrid SCNI/SSCI model offers very good buckling modes. Also, the convergence study using the hybrid SCNI/SSCI meshfree model confirms its good performance in buckling analysis of plate.

Acknowledgements This research was partially supported by JSPS KAKENHI Grant-in-Aid for Scientific Research (A)(15H02328), (B)(15H04212) and (C)(15K06632). T.Q. Bui gratefully acknowledges support in the form of a Grant-in-Aid for Scientific Research (No. 26-04055) - JSPS.

References

1. Common structural rules for bulk carriers and oil tankers (2014) IACS
2. Recommended practice DNV-RP-C201 (2010) Buckling strength of plated structures. DNV
3. Recommended practice DNV-RP-C202 (2013) Buckling strength of shells. DNV
4. Yao T, Astrup OC , Caridis P, Chen YN, Cho SR, Dow RS, Niho O, Rigo P (2000) Ultimate hull girder strength. Proc of the 14th Int Ship and Offshore Struct Congr 321-391
5. Fujikubo M, Kaeding P (2002) New simplified approach to collapse analysis of stiffened plates. Mar Struct 15:251-283
6. Yao T (2003) Hull girder strength. Mar Struct 16:1-13
7. Report of research committee for verification of ISO formulas to evaluate ultimate strength (2011) The Japan Society of Naval Architects and Ocean Engineers
8. Tanaka S, Yanagihara D, Yasuoka A, Harada M, Okazawa S, Fujikubo M, Yao T (2014) Evaluation of ultimate strength of stiffened panels under longitudinal thrust. Mar Struct 36:21-50
9. Pei Z, Iijima K, Fujikubo M, Tanaka S, Okazawa S, Yao T (2015) Simulation on progressive collapse behaviour of whole ship model under extreme waves using idealized structural unit method. Mar Struct 40:104-133
10. Yao, T., Fujikubo, M. (2016) Buckling and ultimate strength of ship and ship-like floating structures, 1st *ed.*. Butterworth-Heinemann
11. Zienkiewicz OC, Taylor RL (2005) The finite element method for solid and structural mechanics, sixth edition. Butterworth-Heinemann
12. Bathe KJ (2007) Finite element procedures. Klaus-Jurgen Bathe
13. Belytschko T, Lu YY, Gu L (1994) Element-free Galerkin Methods. Int J Numer Meth Eng 37:229-256
14. Liu WK, Jun S, Zhang YF (1995) Reproducing kernel particle methods. Int J Numer Meth Fluid 20:1081-1106
15. Liu WK, Jun S, Li S, Adee J, Belytschko T (1995) Reproducing kernel particle methods for structural dynamics. Int J Numer Meth Eng 38:1655-1679
16. Wang D, Chen P (2014) Quasi-convex reproducing kernel meshfree method. Comput Mech 54:689-709
17. Atluri NS, Zhu T (1998) A new meshless local Petrov-Galerkin (MLPG) approach in computational mechanics. Comput Mech 22:117-127

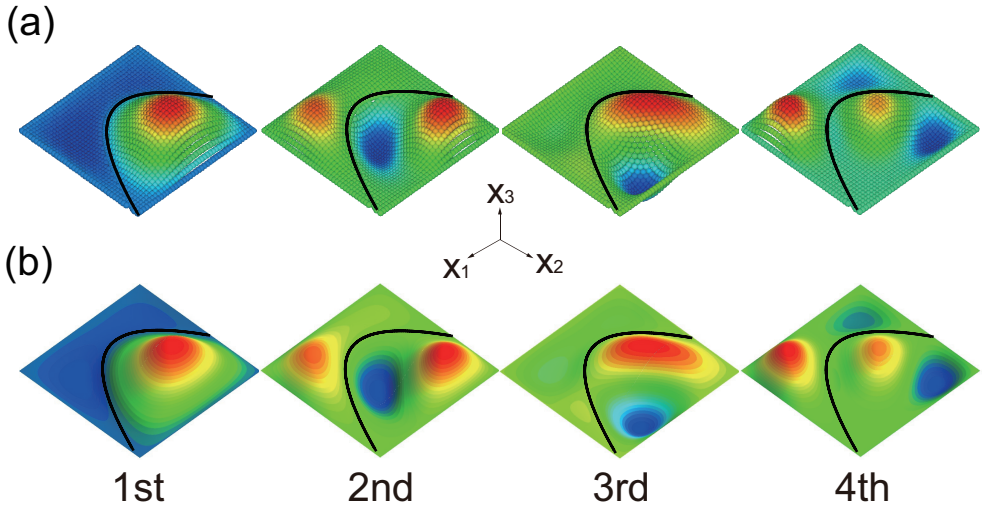

Fig. 10 Comparison of the first four buckling modes of the rectangular plates for Model A **a** Meshfree model. **b** FE model

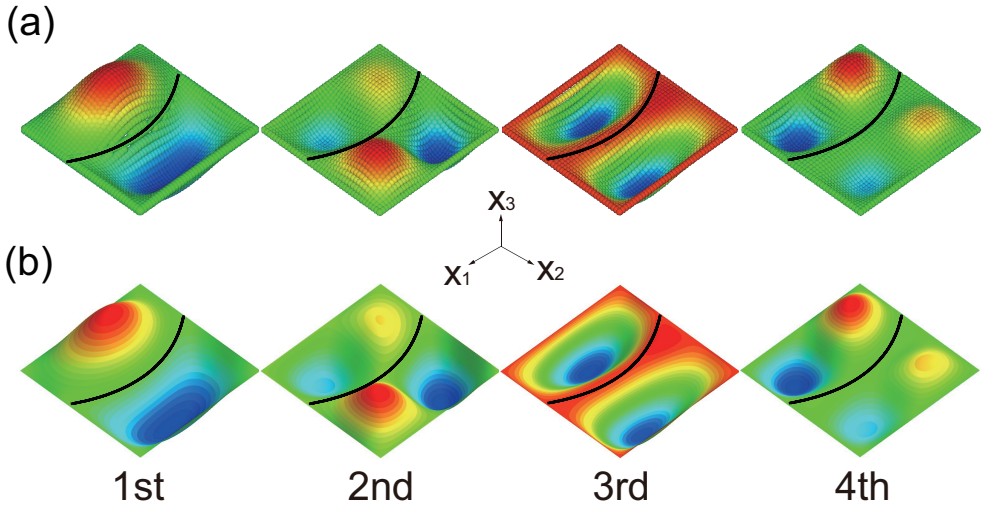

Fig. 11 Comparison of the first four buckling modes of the rectangular plates for Model B **a** Meshfree model. **b** FE model

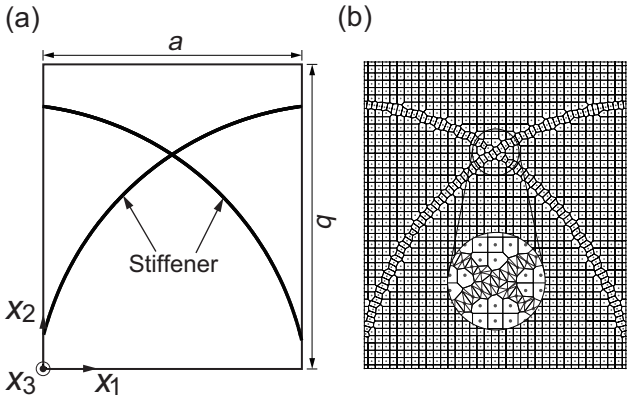

Fig. 12 Rectangular plate with two curved stiffeners. **a** Model C. **b** Meshfree model for Model C

18. Gu L (2003) Moving kriging interpolation and element free Galerkin method. Int J Numer Meth Eng 56:1-11

19. Bui TQ, Nguyen TN, Nguyen-Dang H (2009) A moving Kriging interpolation-based meshless method for numerical simulation of Kirchhoff plate problems. Int J Numer Meth Eng 77:1371-1395

20. Bui TQ, Nguyen MN, Zhang C (2011) A moving Kriging interpolation-based element-free Galerkin method for structural dynamic analysis. Comput Methods Appl Mech Engrg 200:1354-1366

21. Bui TQ, Nguyen MN, Zhang Ch (2011) Buckling analysis of Reissner-Mindlin plates subjected to in-plane edge loads using a shear-locking-free and meshfree method. Eng Anal Bound Elem 35:1038-1053

22. Tanaka S, Okada H, Okazawa S (2012) A wavelet Galerkin method employing B-spline bases for solid mechanics problems without the use of a fictitious domain. Comput Mech 50:35-48

23. Li B, Chen X (2014) Wavelet-based numerical analysis: A review and classification. Finite Elem Anal Des 81:14-31

24. Zhang L, Wang J, Zhou Y-H (2015) Wavelet solution for large deflection bending problems of thin rectangular plates. Arch Appl Mech 85:355-365

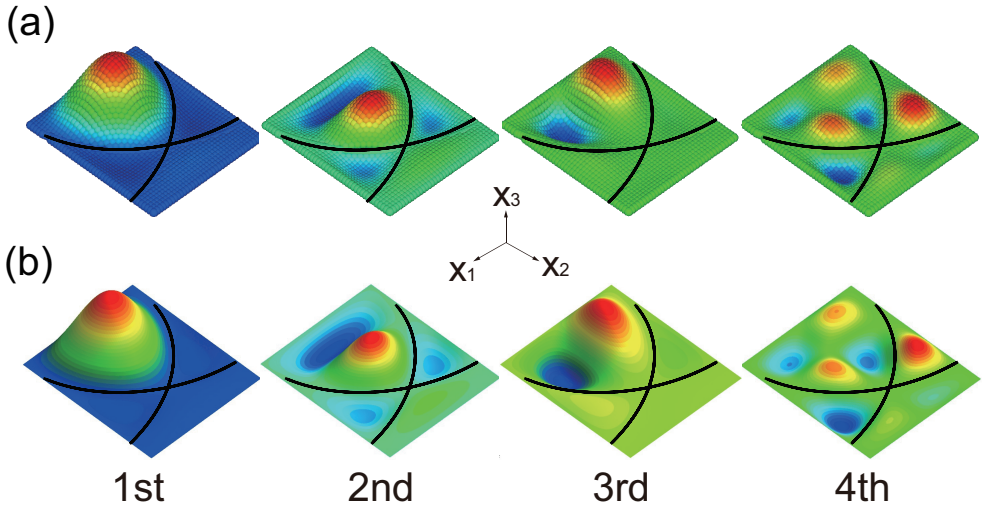

Fig. 13 Comparison of the first four buckling modes of the rectangular plates for Model C **a** Meshfree model. **b** FE model

25. Tanaka S, Suzuki H, Ueda S, Sannomaru S (2015) An extended wavelet Galerkin method with a high-order B-spline for 2D crack problems. Acta Mech 226:2159-2175
26. Tanaka S, Sannomaru S, Imachi M, Hagihara S, Okazawa S, Okada H (2015) Analysis of dynamic stress concentration problems employing spline-based wavelet Galerkin method. Eng Anal Bound Elem 58:129-139
27. Hughes TJR, Cottrell JA, Bazilevs Z (2005) Isogeometric analysis: CAD, finite elements, NURBS, exact geometry and mesh refinement. Comput Methods Appl Mech Engrg 194:4135-4195
28. Shojaee S, Valizadeh N, Izadpanah E, Bui T, Vu TV (2012) Free vibration and buckling analysis of laminated composite plates using the NURBS-based isogeometric finite element method. Compos Struct 94:1677-1693
29. Yu T, Bui TQ, Yin S, Doan DH, Wu CT, Do TV, Tanaka S (2016) On the thermal buckling analysis of functionally graded plates with internal defects using extended isogeometric analysis. Compos Struct 136:684-695
30. Yu T, Yin S, Bui TQ, Xia S, Tanaka S, Hirose S (2016) NURBS-based isogeometric analysis of buckling and free vibration problems for laminated composites plates with complicated cutouts using a new simple FSDT theory and level set method. Thin Wall Struct, 101:141-156
31. Yin S, Yu T, Bui TQ, Zhen X, Tanaka S (2016) In-plane material inhomogeneity of functionally graded plates: A higher-order shear deformation plate isogeometric analysis. Compos B Eng, 106:273-284
32. Wang D, Chen JS (2004) Locking-free stabilized conforming nodal integration for meshfree Mindlin-Reissner plate formulation. Comput Meth Appl Mech Eng 193:1065-1083
33. Chen JS, Wu CT, Yoon S, You Y (2001) A stabilized conforming nodal integration for Galerkin meshfree methods. Int J Numer Meth Eng 50:435-466
34. Chen JS, Yoon S, Wu CT (2002) Non-linear version of stabilized conforming nodal integration for Galerkin meshfree methods. Int J Numer Meth Eng 53:2587-2615
35. http://www.qhull.org/ [accessed 1.1.16]
36. Wang D, Sun Y (2011) A Galerkin meshfree method with stabilized conforming nodal integration for geometrically nonlinear analysis of shear deformable plates. Int J Comput Meth 8:685-703
37. Sadamoto S, Tanaka S, Okazawa S (2013) Elastic large deflection analysis of plates subjected to uniaxial thrust using meshfree Mindlin-Reissner formulation. Comput Mech 52:1313-1330
38. Sadamoto S, Tanaka S, Okazawa S (2014) Buckling analysis of plate with an initial imperfection using RKPM based on convected coordinate system. J Soc Naval Arch Japan 19:169-178 (in Japanese)
39. Wang D, Chen JS. (2008) A Hermite reproducing kernel approximation for thin-plate analysis with sub-domain stabilized conforming integration. Int J Numer Meth Eng 74:368-390
40. Wang D, Peng H (2013) A Hermite reproducing kernel Galerkin meshfree approach for buckling analysis of thin plates. Comput Mech 51:1013-1029
41. Wang D, Lin Z. (2010) Free vibration analysis of thin plates using Hermite reproducing kernel Galerkin meshfree method with sub-domain stabilized conforming integration. Comput Mech 46:703-719
42. Wang D, Lin Z (2011) Dispersion and transient analyses of Hermite reproducing kernel Galerkin meshfree method with sub-domain stabilized conforming integration for thin beam and plate structures. Comput Mech 48:47-63
43. Tanaka S, Sadamoto S, Okazawa S (2012) Nonlinear thin-plate bending analyses using the Hermite reproducing kernel approximation. Int J Comput Meth 9:1240012
44. Wang D, Lin Z (2012) A comparative study on the dispersion properties of HRK and RK meshfree approximations for Kirchhoff plate problem. Int J Comput Meth 9:1240015
45. Chen JS, Wang HP (2000) New boundary condition treatments in meshfree computation of contact problems. Comput Mech 187:441-468
46. Wang D, Chen JS (2006) A locking-free meshfree curved beam formulation with the stabilized conforming nodal integration. Comput Mech 39:83-90
47. Tanaka S, Suzuki H, Sadamoto S, Imachi M, Bui TQ (2015) Analysis of cracked shear deformable plates by an effective meshfree plate formulation. Eng Fract Mech 144:142-157
48. Tanaka S, Suzuki H, Sadamoto S, Bui TQ, Yu TT (2016) *J*-integral evaluation for 2D mixed-mode crack problems employing a meshfree stabilized conforming nodal integraiton method. Comput Mech 58:185-198
49. Tanaka S, Suzuki H, Sadamoto S, Okazawa S, Yu TT, Bui TQ (2016) Accurate evaluation of mixed-mode intensity factors of cracked shear-deformable plates by an en-

riched meshfree Galerkin formulation. Arch Appl Mech 10.1007/s00419-016-1193-x
50. Li S, Liu WK (2004) Meshfree particle methods. Springer, Berlin
51. Timoshenko SP, Gere JM (1988) Theory of elastic stability, 2nd edn. McGraw-Hill, New York
52. Sadamoto S, Tanaka S, Okazawa S (2013) A study for numerical integration technique of plate bending analysis employing meshfree approach. Transactions of JSCES Paper No. 20130008 (in Japanese)
53. Tamijani AY, Kapania RK (2010) Buckling and static analysis of curvilinearly stiffened plates using mesh-free method. AIAA journal 48:2739-2751
54. Shi P, Kapania RK, Dong CY (2015) Vibration and buckling analysis of curvilinearly stiffened plates using finite element method. AIAA journal 53:1319-1335